nature chemical biology

ARTICLES

https://doi.org/10.1038/s41589-020-0602-1

Check for updates

A bioluminescent probe for longitudinal monitoring of mitochondrial membrane potential

Arkadiy A. Bazhin[1], Riccardo Sinisi[1], Umberto De Marchi[2], Aurélie Hermant[2], Nicolas Sambiagio[1], Tamara Maric[1], Ghyslain Budin[1] and Elena A. Goun[1]✉

Mitochondrial membrane potential ($\Delta\Psi_m$) is a universal selective indicator of mitochondrial function and is known to play a central role in many human pathologies, such as diabetes mellitus, cancer and Alzheimer's and Parkinson's diseases. Here, we report the design, synthesis and several applications of mitochondria-activatable luciferin (MAL), a bioluminescent probe sensitive to $\Delta\Psi_m$, and partially to plasma membrane potential ($\Delta\Psi_p$), for non-invasive, longitudinal monitoring of $\Delta\Psi_m$ in vitro and in vivo. We applied this new technology to evaluate the aging-related change of $\Delta\Psi_m$ in mice and showed that nicotinamide riboside (NR) reverts aging-related mitochondrial depolarization, revealing another important aspect of the mechanism of action of this potent biomolecule. In addition, we demonstrated application of the MAL probe for studies of brown adipose tissue (BAT) activation and non-invasive in vivo assessment of $\Delta\Psi_m$ in animal cancer models, opening exciting opportunities for understanding the underlying mechanisms and for discovery of effective treatments for many human pathologies.

Mitochondrial membrane potential ($\Delta\Psi_m$) is an important indicator of mitochondrial function and is crucial for a variety of metabolic processes in both mitochondria and cells. Maintenance of $\Delta\Psi_m$ is fundamental for the growth, differentiation and survival of cells[1–8]. Importantly, $\Delta\Psi_m$ is perturbed in virtually all cases where mitochondrial malfunction contributes to human diseases, such as in diabetes mellitus, cardiovascular, neurodegenerative and neuromuscular diseases, cancer, gastrointestinal disorders and many others[1–8]. Although, in many of these pathologies, it is unclear whether changes in $\Delta\Psi_m$ are a primary cause or a secondary event, the direct involvement of $\Delta\Psi_m$ has been widely confirmed[1–8]. The ability to quantify changes in $\Delta\Psi_m$ is thus extremely important for understanding the molecular mechanisms controlling cell functions and therefore of considerable interest for drug development.

A major obstacle in understanding $\Delta\Psi_m$ function is the absence of sensitive and non-invasive tools. The existing methods for measuring $\Delta\Psi_m$ include fluorescence-activated cell sorting (FACS), confocal microscopy, positron emission tomography (PET) and mass spectrometry (MS)[8–16]. All these methods rely on mitochondria-specific accumulation of fluorescent or radioactive lipophilic cations. Optical imaging reagents remain the most commonly used tools for measuring $\Delta\Psi_m$ in vitro because they are simple to use, cost-effective, provide excellent time resolution and offer a high-throughput alternative to all other modalities in a preclinical setting[9–11]. As a result, reagents such as fluorescent JC-1, TMRM or $DiOC_6$ have been widely utilized to assess changes in the $\Delta\Psi_m$ in many different cell lines[9–11] and even in transparent organisms like *Danio rerio* or *Caenorhabditis elegans*[15,16]. However, currently available fluorescent dyes still have many limitations, including non-specific binding contributing to the overall background signal[9–11] and inhibition of electron transport chain proteins[10], among others. Although many can be overcome by optimizing assay conditions, none of the fluorescent dyes is applicable for $\Delta\Psi_m$ monitoring in non-transparent organisms, for example mice, in a non-invasive manner. At the same time, tissue culture and relatively simple organisms such as zebrafish and are not suitable models for reflecting all the complexity of human pathologies in which $\Delta\Psi_m$ is known to play a central role and for which relevant animal models already exist (for example, cancer, diabetes and Alzheimer's disease). Although potentiometric ^{18}F-based PET tracers can be used to monitor $\Delta\Psi_m$ in virtually all animal models[8,12,13], it is not easy to apply them in a laboratory setting due to the short half-life of the radionuclide (109 min), the requirement for constant access to the cyclotron, and exposure of working personnel and the study subject to ionizing radiation. These shortcomings triggered the development of other non-radioactive alternatives. A non-radioactive $\Delta\Psi_m$-specific probe has been used to monitor $\Delta\Psi_m$ in live animals using sensitive MS[14]. The method is based on $\Delta\Psi_m$-dependent accumulation of two 'click' reagents inside the mitochondria matrix and subsequent formation of a 'Mitoclick' product for which concentration is further assessed by MS. Although the method does not require the use of radioactivity and is quite sensitive, it requires animals to be euthanized and is therefore invasive and suitable only for end-point measurements. Therefore, new tools that overcome these shortcomings and allow sensitive, non-invasive, longitudinal and non-radioactive measurement of $\Delta\Psi_m$ in animals are urgently needed to facilitate our understanding of the underlying mechanisms of these diseases and to accelerate novel drug development.

Here, we have developed a novel 'mitochondria-activatable luciferin' (MAL) probe that allows us to monitor changes in $\Delta\Psi_m$ in a non-invasive, longitudinal fashion both in vitro and in vivo. The approach is based on the combination of a mitochondria-targeted bioorthogonal 'click' reaction and a sensitive bioluminescent imaging (BLI) technique, which is the most sensitive modality in vivo[17–25]. It obviates many of the intrinsic limitations of in vivo fluorescence imaging, such as high tissue-derived autofluorescence and limited tissue penetration. This technology has been successfully applied for visualizing multiple biological processes in small animals[17–25], and many luciferase-expressing animal models where luciferase is present in different organs or in diseased tissues such as

[1]Institute of Chemical Sciences and Engineering, School of Basic Sciences, Swiss Federal Institute of Technology Lausanne (EPFL), Lausanne, Switzerland. [2]Nestlé Research, Lausanne, Switzerland. ✉e-mail: elena.goun@epfl.ch

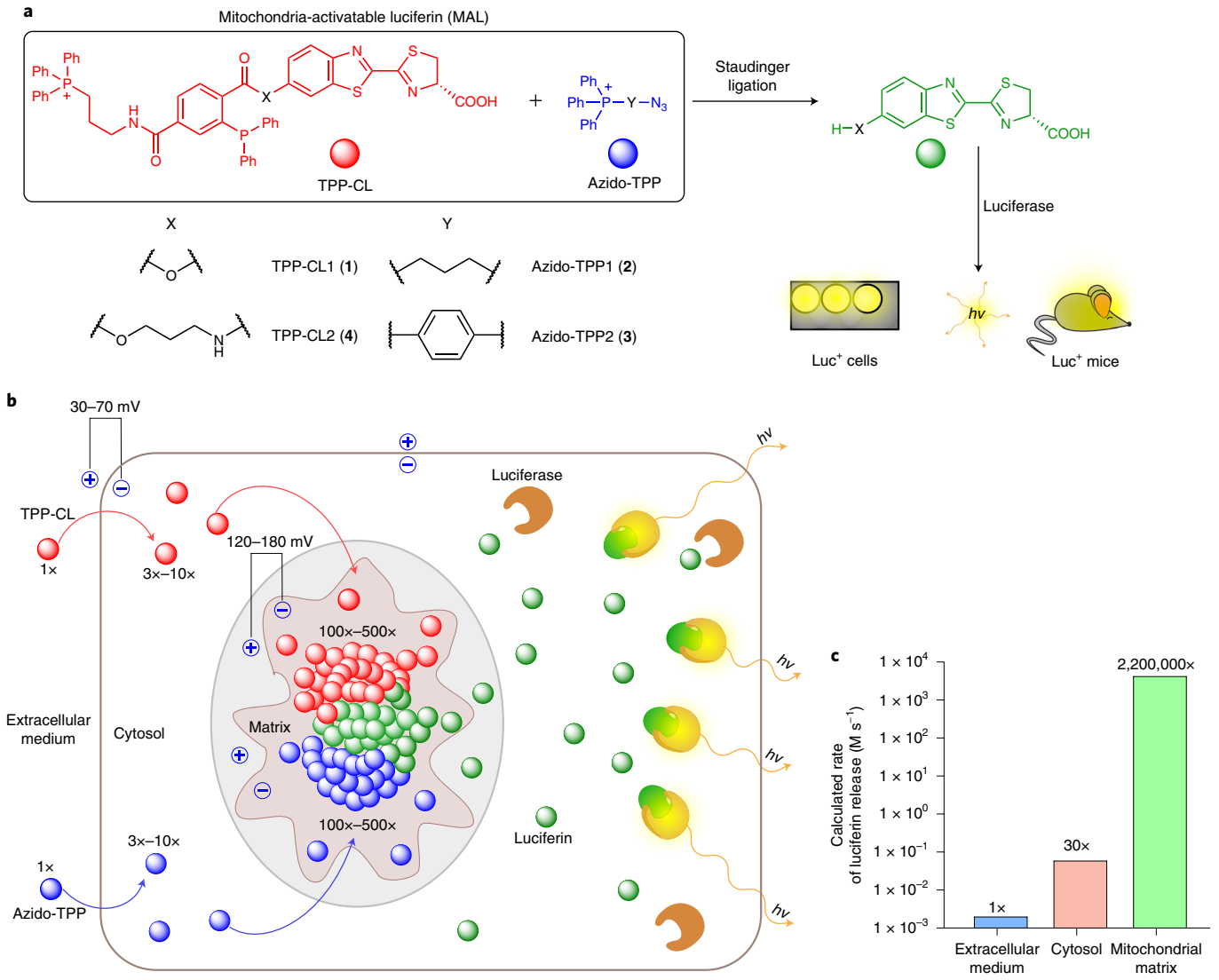

Fig. 1 | Design of the MAL probe. The MAL probe consists of two components, a triphenylphosphine-caged luciferin probe (TPP-CL, red-colored ball) and an azido-triphenylphosphine reagent (azido-TPP, blue-colored ball), both of which are targeted to mitochondria by the triphenylphosphonium (TPP) group. The 'click' reaction (Staudinger ligation) between the reagents results in uncaging of a luciferin derivative (green-colored ball) that, in the presence of luciferase, results in production of photon flux that can be imaged and quantified by a CCD camera or standard plate reader. This technology is easily applicable for non-invasive imaging and monitoring of small changes in $\Delta\Psi_m$, both in vitro and in vivo in a longitudinal fashion. **a**, Chemical reaction of MAL components. **b**, Theoretical illustration of the cellular distribution of MAL reagents in different cellular compartments (extracellular, 1×; cytosolic, 3× to 10×; mitochondrial matrix, 100× to 500×). Relative concentrations were calculated using the Nernst equation (Supplementary Note 1 and Supplementary equation (1)). **c**, Bar graphs representing the calculated reaction rate enhancement in the extracellular space, cytosol and mitochondrial matrix, with the assumptions that the cytoplasmic membrane potential is −45 mV and $\Delta\Psi_m$ is −150 mV (Supplementary Note 1 and Supplementary equations (1)–(4)).

tumors have been reported or are commercially available[23–25], making this imaging modality broadly applicable in preclinical research. However, no BLI-based techniques for probing mitochondrial functions have been reported so far.

Results

Design, synthesis and reactivity studies of MAL probes. The overall design of the MAL probe is depicted in Fig. 1a,b and Supplementary Video 1. The recent development of functional BLI probes for sensing of various biological processes is based on a 'caged' luciferin approach where the firefly luciferin not a substrate for luciferase until it is uncaged by a specific biological event of interest[19–21]. To uncage luciferin, we utilized the bioorthogonal click reaction (Staudinger ligation)[26–28] between an organic azide (azido-TPP) and a caged luciferin triphenylphosphine ester (TPP-CL). Upon this reaction, free luciferin is released, which in turn results in the production of a quantifiable bioluminescent signal catalyzed by luciferase enzyme[29]. This light can be imaged and quantified in a non-invasive real-time fashion using widely available plate readers (in vitro) or sensitive charge-coupled device (CCD) cameras (in vivo). To make release of luciferin $\Delta\Psi_m$-specific, we direct both reagents to mitochondria by using functional handles with lipophilic cations such as triphenylphosphonium (TPP), which have been widely used to successfully deliver various compounds to mitochondria[30–33]. As a result of TPP accumulation, the rate of the Staudinger ligation and subsequent release of luciferin is proportional to the local concentration of both reactants, each of which accumulates ~10^2 and 10^3 times more in the mitochondria than in the cytosol or extracellular matrix, respectively[33] (Fig. 1b and Supplementary Video 1). This dramatic increase in the reagent

concentration results in a significant increase in the rate of luciferin formation (~10^5; Supplementary Note 1 and Supplementary equations (1) to (4)). Closer evaluation of the reaction rate enhancement suggests an exponential relation between the changes in $\Delta\Psi_m + \Delta\Psi_p$ ($\Delta\Psi_p$, plasma membrane potential) and the release of free luciferin (Fig. 1c, Supplementary Fig. 1 and Supplementary equation (4)). We also compared the theoretical contributions of mitochondrial and cytosolic signals to the total signal from a cell and estimated the potential contributions of the extracellular media and cells in the total signal from an assay well (Supplementary Note 1 and Supplementary equations (5)–(7)). These calculations clearly demonstrate that the proposed MAL approach provides the possibility to detect even very small changes in $\Delta\Psi_m$.

To find the best-performing set of reagents for measuring $\Delta\Psi_m$ in live cells and in vivo, we designed and synthesized four different MAL probes (Supplementary Table 1 and Supplementary Notes 2 and 3)[1–8,25,34–36]. The MAL1 probe consists of a combination of TPP-CL1 (**1**), which is a caged luciferin phosphine molecule, and an aliphatic azide (azido-TPP1, **2**), which causes the release of firefly D-luciferin (referred to as 'luciferin') upon undergoing the Staudinger ligation reaction (Fig. 1a and Supplementary Video 1). The MAL2 probe consists of the combination of the same TPP-CL1 molecule and azido-TPP2 (**3**), which was designed to have a lower electron density on the azido group than the original azido-TPP1 compound, leading to a faster reaction rate with TPP-CL1. Because the phenolic hydroxyl group of luciferin is relatively acidic ($pK_a \approx 8$)[37], which makes luciferin a very good leaving group, we anticipated that TPP-CL1 might result in a relatively high background signal arising from the non-specific hydrolysis of luciferin. To address this problem, we designed another TPP-CL molecule where luciferin is linked to TPP via a more stable alkyl ester moiety with a short linker in between (TPP-CL2, **4**; Supplementary Table 1). To make TPP-CL2 more stable, we replaced luciferin in the TPP-CL1 compound with a 3-hydroxypropyl-D-aminoluciferin moiety, which has been reported to produce a higher signal in vivo[34]. The new TPP-CL2 compound was used as a part of the design of the MAL3 and MAL4 probes (Supplementary Table 1).

We next investigated the reaction rate constants for MAL probes. Although the reactions between the MAL1, MAL2 and MAL3 components successfully resulted in the release of their corresponding luciferin derivatives, the reaction between the MAL4 components resulted in the formation of a stable intermediate with no subsequent release of luciferin (Supplementary Note 2). We thus excluded MAL4 from all our subsequent studies. Among the other three MAL probes, MAL1 and MAL2 had the fastest rates of reaction ($0.135 \pm 0.023\ M^{-1}s^{-1}$ and $29.87 \pm 0.84\ M^{-1}s^{-1}$, respectively), which were larger than that of MAL3 ($(1.07 \pm 0.2) \times 10^{-3}\ M^{-1}s^{-1}$) by 100- and 10,000-fold, respectively (Supplementary Fig. 2 and Supplementary Table 1).

Non-invasive $\Delta\Psi_m$ monitoring with MAL probes in vitro. To validate our approach in vitro, we used cells that were stably transfected with the luciferase gene (HT-1080-luc, 4T1-luc and HepG2-luc). The data presented in Supplementary Fig. 3a show a linear increase in light production resulting from treatment of the cells with a 5 µM solution of either the TPP-CL1 or TPP-CL2 probe, indicating the intensity of luciferin release from the TPP-CL molecules due to non-specific hydrolysis. In the case of TPP-CL1, the total photon flux over 1 h was 12-fold higher than for TPP-CL2, which clearly demonstrates that the first molecule is more prone to non-specific hydrolysis (Supplementary Fig. 3b). To identify the best combination of click reagents for producing the highest signal-to-background (S/B) ratio, we treated HT-1080-luc cells with both TPP-CL (5 µM) and the corresponding azido-TPP probes (10 µM) sequentially, with a washing in between to reduce the contribution of extracellular medium to the total signal (Supplementary Note 1 and Supplementary equation (7)), followed by 1 h of continuous signal acquisition. The resulting total photon flux in comparison to the background levels is shown in Supplementary Fig. 4a. All three MAL probes produced robust S/B ratios, with MAL2 and MAL3 probes being superior to MAL1 (S/B ratios of 92 and 89, respectively; Supplementary Fig. 4b).

To investigate whether these concentrations of MAL reagents are non-toxic to cells and do not alter luciferase activity and mitochondrial function, we measured the levels of light output and accumulation of the known mitochondrial probe TMRM at various concentrations of all four TPP-CL and azido-TPP reagents. It was found that azido-TPP2, a component of MAL2, impairs mitochondrial polarization even at 1 µM, while azido-TPP1 does not have any effect at concentrations up to 20 µM (Supplementary Fig. 5). The data also indicate that both TPP-CL1 and TPP-CL2 had no effect on $\Delta\Psi_m$ at concentrations up to 20 µM (Supplementary Fig. 5) and were non-toxic to cells at concentrations up to 100 µM (Supplementary Fig. 6). In addition to the viability assays, we also investigated the effect of the MAL probe on cell respiration, an important parameter of bioenergetic status of the cell. Treatment of HT-1080-luc cells with one of the MAL3 components in the concentration range 1–20 µM demonstrated that TPP-CL2 does not affect basal respiration at concentrations up to 20 µM and azido-TPP1 suppresses respiration at concentrations starting from 20 µM (Supplementary Fig. 7). We then measured the effect of the MAL3 components at typical concentrations used in the in vitro assays on basal respiration in cells over 1 h, the duration of time for all the in vitro experiments. Although no effect on basal respiration was detected when live cells were treated with 5 µM TPP-CL2 (Supplementary Fig. 8a,b), 10 µM azido-TPP1 started to mildly suppress respiration on the 52nd minute of incubation, and after 1 h the suppression remained as low as 5% (Supplementary Fig. 8c,d). Additionally, adenosine triphosphate (ATP) consumption upon luciferin oxidation did not have any

Fig. 2 | In vitro validation of the MAL3 probe for imaging and monitoring of $\Delta\Psi_m$. a, Experimental layout for measurements of $\Delta\Psi_m$ using MAL3 in vitro. **b**,**c**, Comparison of MAL3- and TMRM-based methods for the measurement of mitochondrial depolarization induced by valinomycin. **b**, Concentration-dependent decrease in MAL3 light output resulting from HT-1080-luc cells. *Z′* factor = 0.65. $n = 5$ for 0 µM, $n = 6$ for 0.5 and 1 nM, $n = 3$ for 3–20 nM. **c**, Concentration-dependent decrease in fluorescence intensity in HT-1080-luc cells measured by the TMRM probe. *Z′* factor = 0.22. $n = 6$ for 0–1 nM, $n = 3$ for 3–20 nM. The percentage above each bar represents the decrease in signal compared to control (no valinomycin). **d**,**e**, Comparison of MAL3- and TMRM-based methods for the detection of FCCP-induced depolarization in HT-1080-luc cells. **d**, Effect of FCCP on the signal of MAL3 probe from HT-1080-luc cells. $n = 5$ for 0 µM, $n = 4$ for 0.1 µM, $n = 6$ for 0.3 µM, $n = 3$ for 0.5–3 µM. **e**, Measurement of FCCP-induced depolarization with TMRM assay. $n = 6$ for 0–0.3 µM, $n = 3$ for 0.5–3 µM. **f**,**g**, Comparison of MAL3- and TMRM-based methods for the monitoring of mitochondrial hyperpolarization by nigericin. **f**, Concentration-dependent increase in signal resulting from 4T1-luc cells measured with MAL3. *Z′* factor = 0.83. $n = 6$. **g**, Concentration-dependent increase in fluorescence intensity in 4T1-luc cells measured by TMRM probe. *Z′* factor = 0.3. The numbers above the bars represent the fold increase in signal above the corresponding control group (no nigericin). $n = 10$. Experiments in **b**–**g** were performed independently at least twice. The total photon flux values were obtained by integrating the kinetic curves over 45 min for **b** and **d** and 60 min for **f**. In **b**–**g**, data are presented as mean ± s.d. *n* values represent the number of biologically independent samples in a single experiment. *P* values in **b**,**d**–**g** were calculated by one-way analysis of variance (ANOVA) with Dunnett's multiple comparisons test. *P* values in **c** were calculated by one-way ANOVA with Fisher's least significant difference test. NS, not significant.

influence on $\Delta\Psi_m$ and the adenosine diphosphate (ADP)/ATP ratio at luciferin concentrations up to 10 µM (Supplementary Fig. 9). Because the MAL3 probe demonstrated the highest S/B ratio and its components did not affect cell viability or mitochondrial function at the concentrations used for the assays (10 µM azido-TPP1, 5 µM TPP-CL2), we focused our efforts on investigating the performance of this probe in all further experiments.

In vitro validation of the MAL3 probe. In the next step, we investigated whether the light output from cells incubated with the MAL3 probe correlated with $\Delta\Psi_m$. The outline of the experiment is depicted in Fig. 2a. HT-1080-luc cells were incubated with 5 µM TPP-CL2 in growth medium with or without various $\Delta\Psi_m$ effectors, i.e., valinomycin, carbonyl cyanide 4-(trifluoromethoxy)phenylhydrazone (FCCP) and nigericin[9–11], for 50 min, followed by a washing step and subsequent addition of the azido-TPP1 reagent (10 µM solution in growth medium). The cells were then imaged continuously for 45 min using an IVIS100 CCD camera (PerkinElmer) and the total photon flux was calculated by integration of the area under the corresponding kinetic curve. In the majority of in vitro experiments, we used TMRM as a control because it is a widely used fluorescent reagent and is considered a gold standard in the field of $\Delta\Psi_m$

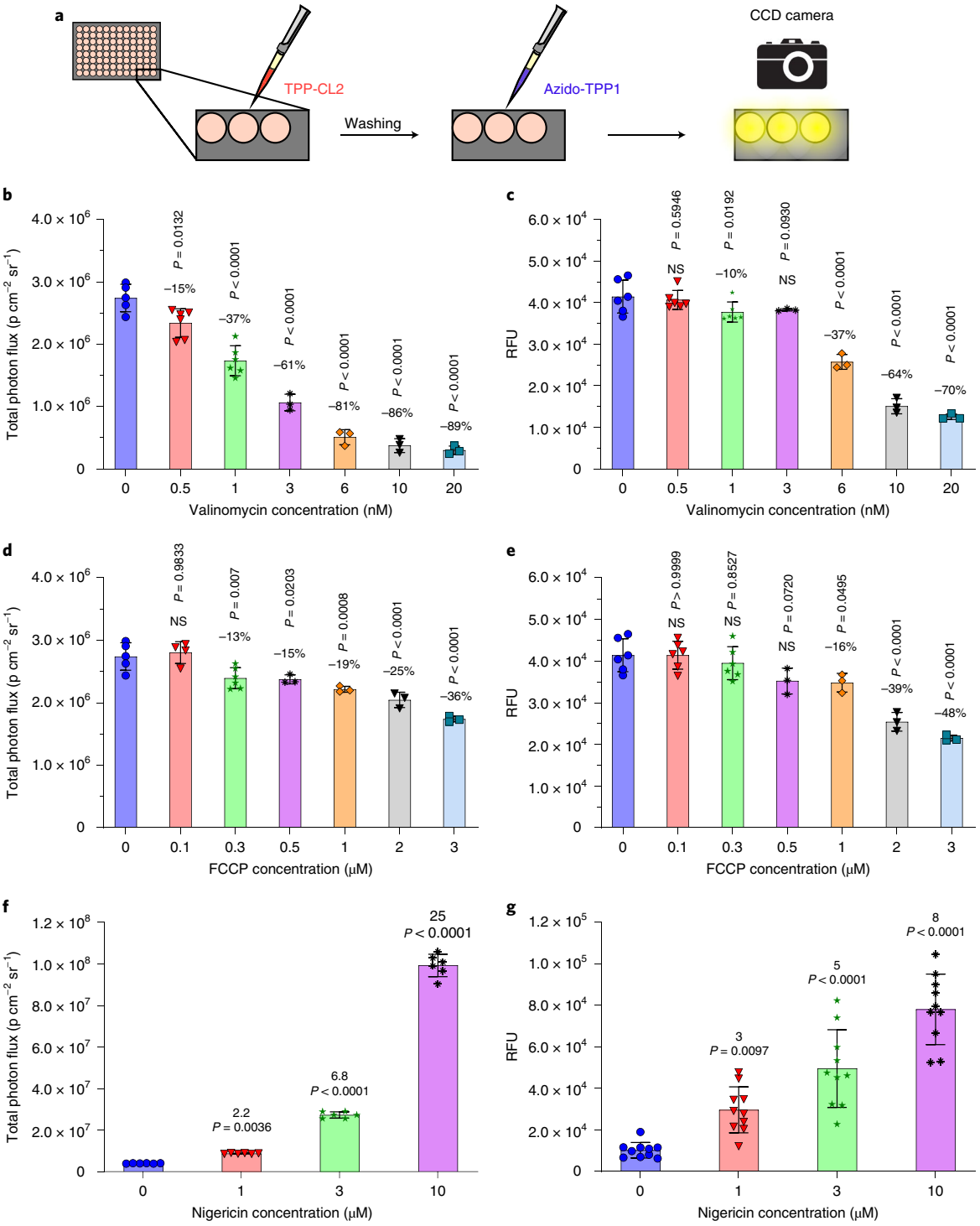

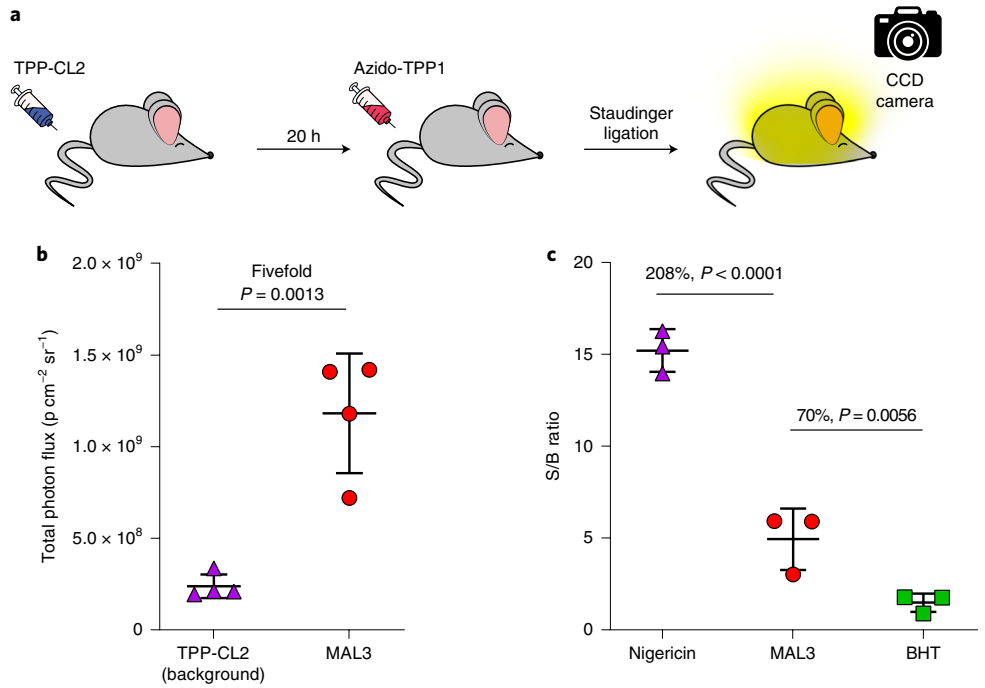

Fig. 3 | In vivo validation of the MAL3 probe for imaging and monitoring of $\Delta\Psi_m$. a, Experimental layout for measurements of $\Delta\Psi_m$-mediated light production in mice using the MAL3 probe. Luciferase-expressing mice first received an i.v. injection of TPP-CL2 followed by an i.p. injection with either azido-TPP1 or PBS (control group) 20 h later, with continuous signal acquisition using a CCD camera for 1 h. **b**, The total photon flux resulting from the MAL3 probe was quantified and plotted against the background (TPP-CL2). The results indicate a fivefold increase in signal upon administration of both MAL3 components. Data are presented as mean ± s.d. ($n = 4$ independent biological replicates). The P value was calculated by two-tailed t-test. **c**, In vivo investigation of the effect of mitochondrial depolarizers (BHT) and hyperpolarizers (nigericin) on signal production with the MAL3 probe. Each point represents the total photon flux from a mouse after administration of MAL3 with or without an effector (see **a**), normalized to the corresponding background (TPP-CL2 ± vehicle for the effector). Data are presented as mean ± s.d. ($n = 3$ independent biological replicates). P values were calculated by one-way ANOVA with Dunnett's multiple comparisons test. Experiments in **b** and **c** were performed independently twice.

in vitro measurements[9–11]. As expected, both the MAL3 and TMRM assays demonstrated a concentration-dependent decrease in signal on increasing the concentrations of FCCP or valinomycin. However, the minimum effective concentration of valinomycin detected with the MAL3 probe was two times lower than that detected with TMRM (0.5 nM versus 1 nM; Fig. 2b,c and Supplementary Fig. 10a). Similar results were observed with FCCP: the minimum effective concentration detected with MAL3 was three times lower than that detected with TMRM (0.3 µM versus 1 µM; Fig. 2d,e and Supplementary Fig. 10b). As expected, the dose-dependent decrease of total photon flux from the MAL3 probe upon valinomycin treatment was exponential, and its nonlinearity was more pronounced compared to TMRM (Supplementary Fig. 11). To further evaluate the assay, we calculated the Z' factor, which is a standard measure of assay reliability[35]. Comparison of Z' factors indicated that the MAL3-based assay was more reliable than the classic TMRM assay (0.65 versus 0.52). No significant effect of FCCP or valinomycin on luciferase activity was detected in the concentration range used for the assay (Supplementary Figs. 12 and 13).

In the next step, we investigated the possibility of detecting the hyperpolarization of mitochondria with the MAL3 probe. For these experiments, we used nigericin, which is an antibiotic known to convert proton gradient (ΔpH) to $\Delta\Psi_m$ (ref. [11]), causing a significant increase in $\Delta\Psi_m$. Therefore, nigericin is particularly efficient in cells where mitochondria have a high ΔpH and low $\Delta\Psi_m$. We first performed an in vitro screen of several cell lines for their response to nigericin by measuring TMRM accumulation and found that HepG2-luc and 4T1-luc were the most appropriate cells lines for testing mitochondrial hyperpolarization (Supplementary Fig. 14). Treatment of these cell lines with the MAL3 probe and increasing concentrations of nigericin also resulted in a robust concentration-dependent increase in bioluminescent signal in both cell lines (Fig. 2f and Supplementary Figs. 15a and 16) with the Z' factor being above 0.8, which indicates the high reliability of the MAL3 assay for $\Delta\Psi_m$ hyperpolarization measurements. Although the same trend was observed in control experiments with TMRM, the reliability of this assay was significantly lower ($Z' < 0.2$) (Fig. 2g and Supplementary Fig. 15b). No significant effect of nigericin on luciferase activity in cells was observed in the concentration range used for this assay (Supplementary Fig. 17).

It is important to note that the total signal of the MAL3 probe as well as any other probe based on redistribution of lipophilic cations, for example TMRM, JC1 and $DiOC_6$, depends on both $\Delta\Psi_m$ and $\Delta\Psi_p$ (refs. [9–11]). Therefore, we decided to quantify the contribution of $\Delta\Psi_p$ to the signal of MAL3 and TMRM by comparing their signals from HT-1080-luc cells in media with low (5.77 mM) and high (125 mM) concentrations of K^+ ions (Supplementary Table 2). Our results indicated that, in these conditions, the signal from MAL3 was 55% lower compared to low-K^+ medium (Supplementary Fig. 18) and that the decrease was very similar to that obtained with TMRM (61%, Supplementary Fig. 19), a commonly used probe for measurements of $\Delta\Psi_m$ in vitro, demonstrating close similarities between the two probes with respect to the influence of $\Delta\Psi_p$ on their resulting signals.

Next, we decided to further investigate the effect of FCCP, valinomycin and nigericin on the level of $\Delta\Psi_p$ by using a membrane potential evaluation assay kit (Molecular Devices) and high-potassium medium as a positive control. Treatment of live HT-1080-luc cells with FCCP, valinomycin and nigericin at the concentrations used in the MAL3 assays resulted in only minor changes of $\Delta\Psi_p$ compared

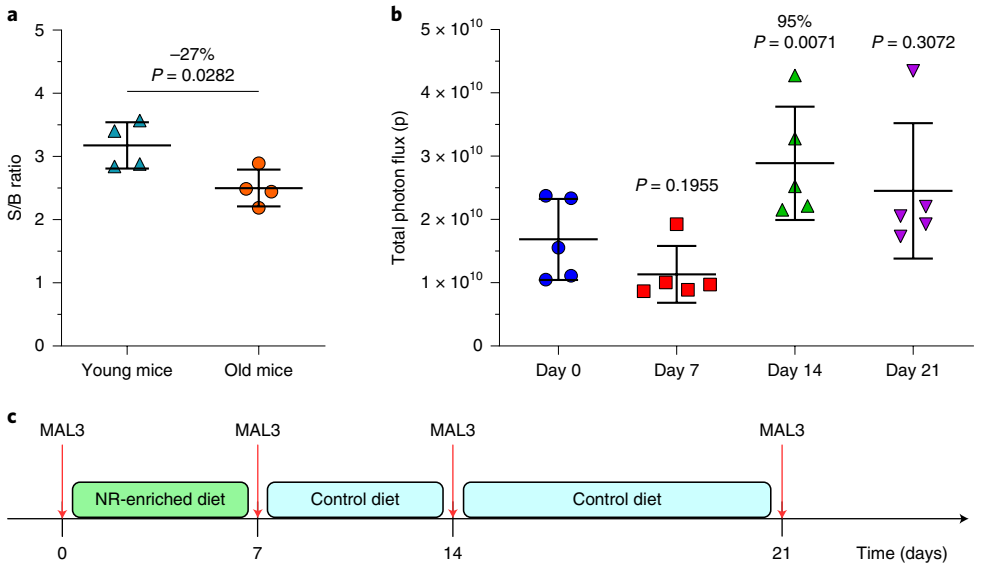

Fig. 4 | Application of the MAL3 probe for monitoring $\Delta\Psi_m$ in young and old mice and investigation of the effect of NR-enriched diet on $\Delta\Psi_m$ in old mice. a, Non-invasive in vivo monitoring of $\Delta\Psi_m$ in 'young' (12 weeks) versus 'old' (65 weeks) FVB-luc$^+$ female mice. Data are presented as mean ± s.d., $n = 4$ independent biological replicates. The P value was calculated by two-tailed t-test. **b**, Monitoring of $\Delta\Psi_m$ in old mice (90–95 weeks, $n = 5$) during the time course of the experiment with the NR-enriched diet. Each point represents the whole-body light output from a mouse resulting from administration of the MAL3 probe. Data are presented as mean ± s.d., $n = 5$ independent biological replicates. P values were calculated by paired one-way ANOVA with Greenhouse–Geisser correction and Dunnett's multiple comparisons test. **c**, Experimental outline for monitoring $\Delta\Psi_m$ in old mice fed with the NR-enriched diet shown in **b**. The experiments presented in **a** and **b** were repeated twice.

to the effect of high-potassium medium (60 mM) (Supplementary Fig. 20) and these data were consistent with previous reports[36]. To complete in vitro validation of the MAL3 probe, we tested the effect of electron transport chain (ETC) inhibitors on the MAL3 signal, because they are known to be selective for mitochondria and do not affect $\Delta\Psi_p$. We found that treatment of HT-1080-luc cells with a combination of 10 µM antimycin A and 7 µM oligomycin (inhibitors of complex 3 and ATP-synthase, respectively)[38] resulted in a 66% decrease in MAL3 signal and a 68% decrease in TMRM signal (Supplementary Fig. 21), further indicating the similarity between the two probes with respect to the influence of $\Delta\Psi_p$ signals.

Non-invasive monitoring of $\Delta\Psi_m$ with MAL3 probes in vivo. To assess the application of the MAL3 probe for non-invasive $\Delta\Psi_m$ monitoring in live animals, we used healthy transgenic mice in which firefly luciferase is ubiquitously expressed under the β-actin promoter (further abbreviated as 'FVB-luc$^+$' mice)[24]. To avoid the reaction between MAL components occurring in the blood, the animals were injected with TPP-CL2 probe 20 h before administration of the azido-TPP1 reagent (Fig. 3a). Indeed, multiple previous in vivo studies have demonstrated that TPP cations are washed out from the bloodstream and accumulate inside the mitochondria within a period of ~20 h (refs. [30–33]). Two groups of FVB-luc$^+$ mice ($n = 4$) received an intravenous (i.v.) injection of TPP-CL2 followed by intraperitoneal (i.p.) injection of azido-TPP or vehicle 20 h later, with continuous signal acquisition using a CCD camera for 1 h. By comparing the resulting total photon flux (area under the curve, AUC) for both groups, we observed a robust S/B ratio (fivefold, Fig. 3b).

To investigate the $\Delta\Psi_m$ signal specificity, we first used butylated hydroxytoluene (BHT, E321), a well-known antioxidant used in the food industry because of its low toxicity. Previous studies on isolated mitochondria showed that BHT acts as a mild uncoupler; that is, it depolarizes mitochondria and increases the basal oxygen consumption rate in vitro[39]. Our results demonstrate that oral gavage of BHT to FVB-luc$^+$ mice at concentrations of 60 mg kg^{-1} leads to a significant increase of oxygen consumption rate (OCR), which is typically expected for a classical uncoupler (Supplementary Fig. 22a). We also measured the effect of nigericin, a widely used $\Delta\Psi_m$ hyperpolarizer[11], on OCR in mice and observed that it effectively suppresses respiration (Supplementary Fig. 22b), which is in agreement with previously published data[40].

To test the effect of BHT on the light output of the MAL3 probe, we used three groups of mice ($n = 3$), which were first injected i.v. with TPP-CL2 solution as described above. Mice in group 1 then received an oral gavage of BHT solution in corn oil (60 mg kg^{-1}), whereas those in groups 2 and 3 received only corn oil. After 20 h, mice in groups 1 and 2 were injected i.p. with azido-TPP1, whereas those in group 3 (background) were injected with vehicle only (PBS buffer). The total photon flux resulting from all three groups was integrated over 1 h and plotted as the S/B ratio of the signal obtained from the MAL3 BHT-treated group (group 1) or the group treated with MAL3 alone (group 2) normalized to the signal from the background (group 3, TPP-CL2 only). The results indicate a significant decrease (70%, Fig. 3c) in MAL3 signal upon BHT treatment, demonstrating non-invasive and non-radioactive imaging of $\Delta\Psi_m$ depolarization in live mice.

To determine whether the MAL3 probe can be used to non-invasively detect $\Delta\Psi_m$ hyperpolarization in live mice, we repeated the same experiment using nigericin instead of BHT. The results presented in Fig. 3c demonstrate a 208% increase in light output in the mice treated with nigericin in comparison to the mice treated with vehicle only (control), and the data are in agreement with previous in vitro results (Fig. 2f). Together, these data indicate the $\Delta\Psi_m$ specificity of the signal resulting from the MAL3 probe and represent a first example of non-invasive and non-radioactive imaging of $\Delta\Psi_m$ in live mice, opening a wide range of opportunities to study this important parameter in various biological settings, such as animal models of human disease.

Detection of age-related mitochondria depolarization. Next, we decided to apply the MAL3 probe to measure $\Delta\Psi_m$ changes associated with age in young versus old mice. To perform this experiment,

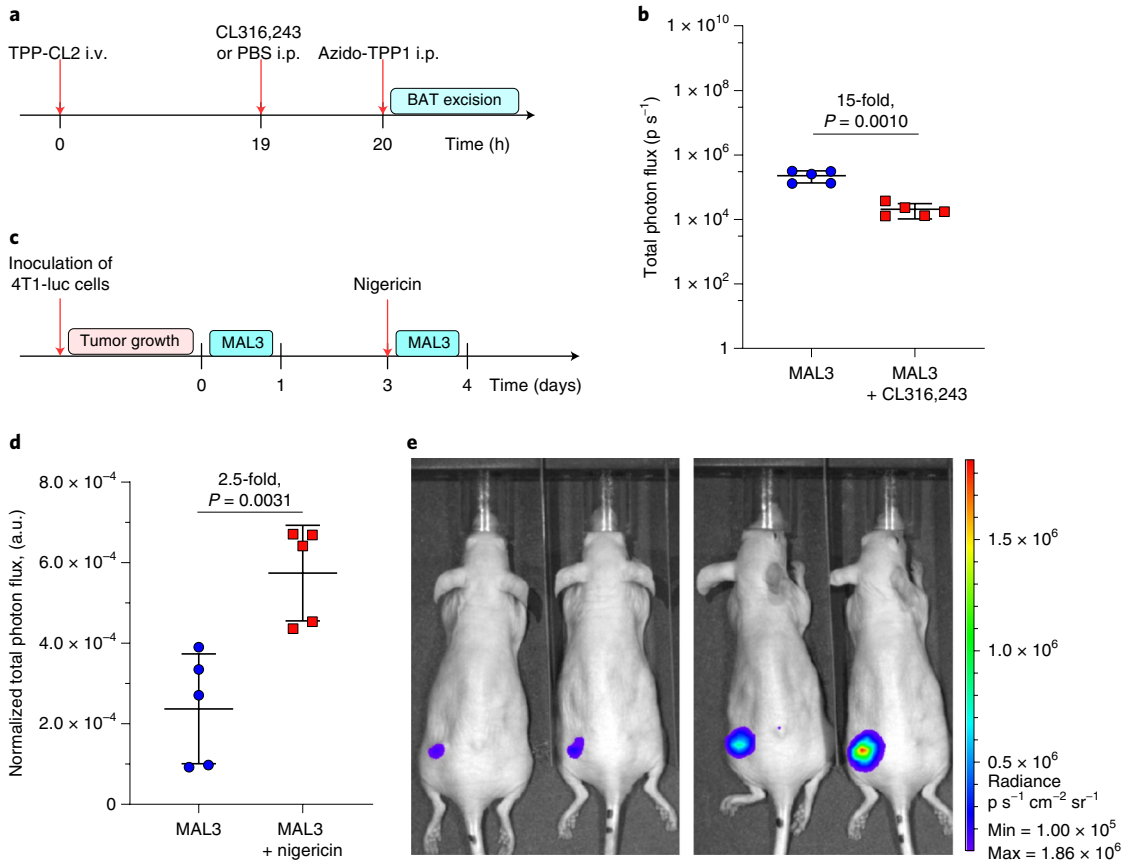

Fig. 5 | Application of MAL3 for monitoring $\Delta\Psi_m$ in BAT and tumor-bearing mice in vivo. a, Experimental layout for the measurements of mitochondrial depolarization in BAT induced by CL316,243 compound. **b**, Total photon flux resulting from excised BAT tissue in control versus CL316,243-treated mice. Data are presented as mean ± s.d. ($n = 5$ independent biological replicates in a single experiment). The P value was calculated by two-tailed t-test. **c**, Experimental outline of the nigericin-induced mitochondrial hyperpolarization experiment in cancer-bearing 4T1-luc tumor xenografts in Swiss nude mice. **d**, Total photon flux from cancer-bearing animals after administration of the MAL3 probe with or without nigericin ($n = 5$ independent biological replicates in a single experiment). Data are presented as mean ± s.d. The P value was calculated by two-tailed t-test. **e**, Representative images of Swiss nude mice bearing 4T1-luc tumor xenografts administered with either MAL3 only (left) or MAL3 with nigericin (right). All presented experiments were repeated twice.

we compared 12-week-old FVB-luc$^+$ mice ('young' group) with 65-week-old mice ('old' group) of the same strain ($n = 4$). On the first day of the experiment, all mice received i.v. injections of TPP-CL2 and were placed back in their cages. After 20 h, the mice were imaged for 30 min using a CCD camera, followed by an i.p. injection of azido-TPP1 and subsequent imaging for another 40 min. The total photon flux resulting from the injection of azido-TPP1 was normalized to the total photon flux resulting from the injection of TPP-CL2 (background) to take into account differences in weight and optical properties (light absorption and scattering) of mice. The results depicted in Fig. 4a demonstrate a 27% decrease in the S/B ratio resulting from old mice. We also determined the contribution of other factors that may affect the MAL3 signal in vivo, such as luciferase activity (Supplementary Fig. 23), clearance of TPP-CL2 (Supplementary Fig. 24) and relative mitochondrial content in various organs of young versus old mice (Supplementary Fig. 25). The results indicate no significant differences in these parameters in the strain of mice used for the experiments. Therefore, our data support the theory that aging results in a significant decrease in $\Delta\Psi_m$ and demonstrate a first example of direct non-invasive measurements of $\Delta\Psi_m$ in young versus old mice.

Effect of NR-enriched diet on $\Delta\Psi_m$ in old living mice. NR is a form of vitamin B3, which has recently been the subject of many investigations and multiple clinical trials due to its beneficial effects on energy metabolism and neuroprotection[41–43]. However, its mechanism of action is not completely understood due to the lack of non-invasive tools. In particular, nothing is known about its effects on $\Delta\Psi_m$ in old mice. To investigate this, we performed non-invasive longitudinal measurements of $\Delta\Psi_m$ using the MAL3 probe in old FVB-luc$^+$ mice (90–95 weeks, $n = 5$) that were kept on an NR-rich diet for one week. The concentration of NR in the diet was equivalent to 0.24% of mixture mass, resulting in a dose of 400 mg kg^{-1} d^{-1}, which has been shown previously to have beneficial effects on metabolism and aging[42].

The results and overall design of the study are outlined in Fig. 4b,c. Measurements of the MAL3 signal on days 0 and 7 demonstrate that seven days of the NR-enriched diet led to a non-significant change in $\Delta\Psi_m$. However, on day 14 of the study, the MAL3 signal rose by 95% (Fig. 4b) compared to day 0. At the same time, no increase in the MAL3 signal was observed in the control group of mice that received regular diet (Supplementary Fig. 27). Subsequent measurements of the MAL3 signal on day 21 of the experiment (two weeks of washout period) indicated that the MAL3 signal had returned to pretreatment levels (day 0).

To measure the potential contribution of mitobiogenesis, we repeated the NR-enriched diet experiment on another group of old mice (90 weeks, $n = 3$) and quantified the mitochondrial-to-nuclear-DNA ratio at days 0, 7 and 14 in various organs (mtco-1/atp-5 ratio, Supplementary Table 2). The results presented in the Supplementary Fig. 26 clearly demonstrate that NR treatment had no significant effect on the

mitochondrial-to-nuclear-DNA ratio. Therefore, the increase in light production from the MAL3 probe as the result of NR treatment of old mice is most probably due to an increase in $\Delta\Psi_m$. To evaluate the potential elevation of activity or expression of luciferase and increase of ATP level, we monitored luciferase activity throughout the study by injecting a high dose of luciferin and quantifying the resulting light emission (Supplementary Fig. 28). No statistically significant change in signal was observed after feeding mice with an NR-enriched diet, further confirming that the differences in MAL3 signal between the groups are most probably due to the biological action of NR.

Measurements of mitochondria uncoupling in BAT. Activation of brown and beige adipocytes has significant potential for the efficient management of many metabolic disorders, such as type 2 diabetes, abnormal lipid metabolism and obesity[5,44–46]. However, mitochondrial depolarization of activated brown adipocytes was demonstrated only in cultured cells. To investigate the applicability of the MAL3 probe for BAT-specific assessment of $\Delta\Psi_m$, we decided to measure changes in the MAL3 signal upon administration of β_3-adrenergic agonists such as CL316,243 (CL) directly in live FVB-luc$^+$ mice (Fig. 5a). Two groups of 15-week-old FVB-luc$^+$ mice ($n=5$) were injected i.v. with TPP-CL2, followed by i.p. injection of CL solution (1 mg kg^{-1}) or vehicle alone 19 h later. After that, the mice from both groups were i.p. injected with azido-TPP1 solution followed by euthanasia and isolation of BAT 50 min post-injection to ensure selectivity of the signal for BAT. We observed a 15-fold decrease in signal from the BAT of mice treated with CL compound in comparison to the PBS-treated control group (Fig. 5b). Importantly, these results are in agreement with the data previously obtained in cultured live adipose cells and isolated mitochondria from BAT and clearly demonstrate that the MAL3 probe represents a powerful tool for elucidating new mechanisms responsible for mitochondrial BAT uncoupling.

Non-invasive monitoring of $\Delta\Psi_m$ in an animal cancer model. Mitochondria are known to play an important role in cancer biology, and screening for mitochondria-specific uncouplers in tumors is a new promising area of anticancer drug discovery[1,7,8,47]. Moreover, elegant recent work by the Shackelford group have revealed distinct functional mitochondrial heterogeneity within subtypes of lung tumors, further emphasizing the importance of non-invasive functional profiling of $\Delta\Psi_m$ in vivo[5]. To investigate the applicability of the MAL3 probe for non-invasive monitoring of $\Delta\Psi_m$ in tumor animal models, we injected 4T1-luc cells subcutaneously in Swiss nude mice. To modulate $\Delta\Psi_m$ we used nigericin, because we have previously observed a substantial increase of MAL3 signal in 4T1-luc cells in vitro and in healthy FVB-luc$^+$ mice. The outline of the experiment is shown in Fig. 5c. To minimize deviation between tumors we applied MAL3 probe twice on the same tumor-bearing animal before and after nigericin administration. The route of administration and concentrations of MAL3 probe components were the same as described in all the previous in vivo experiments (see Methods for more details). We observed a twofold increase in total photon flux from the tumors of mice treated with nigericin (Fig. 5d,e). Because multiple luciferase-expressing cancer models exist[47], these results demonstrate the high utility of the MAL3 probe for cancer research, providing an opportunity for non-invasive, longitudinal studies of $\Delta\Psi_m$ in living animals using sensitive and non-radioactive BLI.

Discussion

Mitochondria play a central role in multiple biological processes, and their dysfunction is involved in many human diseases where it is not possible to mimic their complexity in cell cultures[1–8]. Although $\Delta\Psi_m$ is one of the main indicators of mitochondrial function, no tools exist for the sensitive, non-invasive, longitudinal and non-radioactive imaging and monitoring of $\Delta\Psi_m$ both in vitro and in vivo. This issue is a major obstacle to our understanding of the role of this important mitochondrial function in a range of important human pathologies, making the drug discovery process complex and less efficient. Here, we describe a novel MAL-based approach for monitoring $\Delta\Psi_m$ that is based on a combination of sensitive BLI and novel chemical biology tools.

The novel MAL3 tool has many advantages over existing methods for monitoring $\Delta\Psi_m$. The major advantage over fluorescent-based methods is its applicability for in vivo experiments due to the absence of autoluminescence and the ability to obtain a strong signal, even from deep tissues. Unlike the end-point MS-based method 'Mitoclick'[14], the novel MAL3 approach is non-invasive, less laborious and suitable for longitudinal in vivo monitoring of $\Delta\Psi_m$. In contrast to voltage-sensitive short-lived radiotracers for PET[8,12,13], the new tool does not include the generation and use of radioactive compounds, which makes it more cost-effective and safe. However, PET radiotracers containing ^{18}F are certainly able to provide better spatial resolution in vivo because all biological tissues are transparent to gamma rays. The main limitation of the MAL3 probe is the necessity of using luciferase-expressing animals or cells. However, this 'shortcoming' could also be viewed as a big advantage of the new method because the combination of the MAL3 probe and organ- or tissue-specific luciferase expression could be utilized as a powerful tool to investigate changes in $\Delta\Psi_m$ in particular tissues of interest. We successfully demonstrated such an application in cancer-bearing mice, where luciferase expression was selectively engineered only in cancer tissues. Also, many of the other limitations of the MAL3 tool are the same as for PET- or MS-based methods (nonlinearity of the signal and its dependence on factors other than $\Delta\Psi_m$, such as $\Delta\Psi_p$, clearance of a probe and tissue perfusion, as well as mitochondrial volume and density).

In conclusion, the MAL3 probe is an example of a tool that can be used for non-invasive longitudinal imaging of $\Delta\Psi_m$ both in vitro and in vivo using a sensitive and non-radioactive optical imaging modality (BLI). In addition, the probe is more sensitive than previously reported fluorescent methods (TMRM) in cell-based assays. Although fluorescent methods are superior to BLI in terms of time resolution, they are applicable only for optically transparent organisms, such as *C. elegans* and zebrafish[15,16]. The novel MAL3 approach can be used in mammals, which offer many more relevant models of human pathologies such as cancer, diabetes and Alzheimer's and Parkinson's diseases[1–8,25,48–50]. We successfully demonstrated applications of MAL3 for the non-invasive in vivo detection of $\Delta\Psi_m$ upon aging and monitoring of tumor $\Delta\Psi_m$ in response to treatment. In addition, we showed that the MAL3 probe can be used for the evaluation of changes in $\Delta\Psi_m$ upon BAT stimulation in live mice. Owing to its non-toxic and non-radioactive nature, this novel technology also allows the monitoring of animals over the course of an experiment in a longitudinal fashion. We used this important feature of the MAL3 tool to demonstrate the effect of an NR-enriched diet on $\Delta\Psi_m$ levels in old mice, thereby revealing another fascinating aspect of the biological mechanism of action of this interesting biomolecule. Given the central role of $\Delta\Psi_m$ in many diseases, this new tool lays an important foundation for the field of drug discovery of novel $\Delta\Psi_m$ modulators and identification of the underlying mechanisms of human pathologies.

Online content

Any methods, additional references, Nature Research reporting summaries, source data, extended data, supplementary information, acknowledgements, peer review information; details of author contributions and competing interests; and statements of data and code availability are available at https://doi.org/10.1038/s41589-020-0602-1.

Received: 31 May 2019; Accepted: 29 June 2020;
Published online: 10 August 2020

References

1. Herst, P. M., Rowe, M. R., Carson, G. M. & Berridge, M. V. Functional mitochondria in health and disease. *Front. Endocrinol. (Lausanne)* **8**, 296 (2017).
2. Duchen, M. R. Mitochondria in health and disease: perspectives on a new mitochondrial biology. *Mol. Aspects Med.* **25**, 365–451 (2004).
3. Wang, Y., Xu, E., Musich, P. R. & Lin, F. Mitochondrial dysfunction in neurodegenerative diseases and the potential countermeasure. *CNS Neurosci. Ther.* **25**, 816–824 (2019).
4. Zorova, L. D. et al. Mitochondrial membrane potential. *Anal. Biochem.* **552**, 50–59 (2018).
5. Momcilovic, M. et al. In vivo imaging of mitochondrial membrane potential in non-small-cell lung cancer. *Nature* **575**, 380–384 (2019).
6. Lee, J. H. et al. The role of adipose tissue mitochondria: regulation of mitochondrial function for the treatment of metabolic diseases. *Int. J. Mol. Sci.* **20**, 4924 (2019).
7. Vyas, S., Zaganjor, E. & Haigis, M. C. Mitochondria and cancer. *Cell* **166**, 555–566 (2016).
8. Weinberg, S. E. & Chandel, N. S. Targeting mitochondria metabolism for cancer therapy. *Nat. Chem. Biol.* **11**, 9–15 (2015).
9. Perry, S. W., Norman, J. P., Barbieri, J., Brown, E. B. & Gelbard, H. A. Mitochondrial membrane potential probes and the proton gradient: a practical usage guide. *Biotechniques* **50**, 98–115 (2011).
10. Rottenberg, H. & Wu, S. Quantitative assay by flow cytometry of the mitochondrial membrane potential in intact cells. *Biochim. Biophys. Acta* **1404**, 393–404 (1998).
11. Gerencser, A. A. et al. Quantitative measurement of mitochondrial membrane potential in cultured cells: calcium-induced de- and hyperpolarization of neuronal mitochondria. *J. Physiol.* **590**, 2845–2871 (2012).
12. Madar, I. et al. Characterization of uptake of the new PET imaging compound F-18-fluorobenzyl triphenyl phosphonium in dog myocardium. *J. Nucl. Med.* **47**, 1359–1366 (2006).
13. Kim, D. Y. et al. Evaluation of a mitochondrial voltage sensor, (18F-fluoropentyl)triphenylphosphonium cation, in a rat myocardial infarction model. *J. Nucl. Med.* **53**, 1779–1785 (2012).
14. Logan, A. et al. Assessing the mitochondrial membrane potential in cells and in vivo using targeted click chemistry and mass spectrometry. *Cell Metab.* **23**, 379–385 (2016).
15. Gaskova, D., DeCorby, A. & Lemire, B. D. DiS-C-3(3) monitoring of in vivo mitochondrial membrane potential in *C. elegans*. *Biochem. Biophys. Res. Commun.* **354**, 814–819 (2007).
16. Sasagawa, S. et al. In vivo detection of mitochondrial dysfunction induced by clinical drugs and disease-associated genes using a novel dye ZMJ214 in zebrafish. *ACS Chem. Biol.* **11**, 381–388 (2016).
17. Massoud, T. F. & Gambhir, S. S. Molecular imaging in living subjects: seeing fundamental biological processes in a new light. *Gene Dev.* **17**, 545–580 (2003).
18. Sweeney, T. J. et al. Visualizing the kinetics of tumor-cell clearance in living animals. *Proc. Natl Acad. Sci. USA* **96**, 12044–12049 (1999).
19. Mezzanotte, L., van 't Root, M., Karatas, H., Goun, E. A. & Lowik, C. In vivo molecular bioluminescence imaging: new tools and applications. *Trends Biotechnol.* **35**, 640–652 (2017).
20. Rathbun, C. M. & Prescher, J. A. Bioluminescent probes for imaging biology beyond the culture dish. *Biochemistry* **56**, 5178–5184 (2017).
21. Su, T. A., Bruemmer, K. J. & Chang, C. J. Caged luciferins for bioluminescent activity-based sensing. *Curr. Opin. Biotechnol.* **60**, 198–204 (2019).
22. Maric, T. et al. Bioluminescent-based imaging and quantification of glucose uptake in vivo. *Nat. Methods* **16**, 526–532 (2019).
23. Zagozdzon, A. M. et al. Generation of a new bioluminescent model for visualisation of mammary tumour development in transgenic mice. *BMC Cancer* **12**, 209 (2012).
24. Cao, Y. A. et al. Shifting foci of hematopoiesis during reconstitution from single stem cells. *Proc. Natl Acad. Sci. USA* **101**, 221–226 (2004).
25. Manni, I., de Latouliere, L., Gurtner, A. & Piaggio, G. Transgenic animal models to visualize cancer-related cellular processes by bioluminescence imaging. *Front. Pharmacol.* **10**, 235 (2019).
26. Saxon, E. & Bertozzi, C. R. Cell surface engineering by a modified Staudinger reaction. *Science* **287**, 2007–2010 (2000).
27. Myers, E. L. & Raines, R. T. A phosphine-mediated conversion of azides into diazo compounds. *Angew. Chem. Int. Ed.* **48**, 2359–2363 (2009).
28. Sundhoro, M., Jeon, S., Park, J., Ramstrom, O. & Yan, M. Perfluoroaryl azide Staudinger reaction: a fast and bioorthogonal reaction. *Angew. Chem. Int. Ed.* **56**, 12117–12121 (2017).
29. Cohen, A. S., Dubikovskaya, E. A., Rush, J. S. & Bertozzi, C. R. Real-time bioluminescence imaging of glycans on live cells. *J. Am. Chem. Soc.* **132**, 8563–8565 (2010).
30. Murphy, M. P. Targeting lipophilic cations to mitochondria. *Biochim. Biophys. Acta* **1777**, 1028–1031 (2008).
31. Prime, T. A. et al. A mitochondria-targeted S-nitrosothiol modulates respiration, nitrosates thiols, and protects against ischemia-reperfusion injury. *Proc. Natl Acad. Sci. USA* **106**, 10764–10769 (2009).
32. Jameson, V. J. A. et al. Synthesis of triphenylphosphonium vitamin E derivatives as mitochondria-targeted antioxidants. *Tetrahedron* **71**, 8444–8453 (2015).
33. Ross, M. F. et al. Lipophilic triphenylphosphonium cations as tools in mitochondrial bioenergetics and free radical biology. *Biochemistry (Mosc.)* **70**, 222–230 (2005).
34. Woodroofe, C. C. et al. *N*-alkylated 6′-aminoluciferins are bioluminescent substrates for Ultra-Glo and QuantiLum luciferase: new potential scaffolds for bioluminescent assays. *Biochemistry* **47**, 10383–10393 (2008).
35. Zhang, J. H., Chung, T. D. Y. & Oldenburg, K. R. A simple statistical parameter for use in evaluation and validation of high throughput screening assays. *J. Biomol. Screen.* **4**, 67–73 (1999).
36. Nicholls, D. G. Simultaneous monitoring of ionophore- and inhibitor-mediated plasma and mitochondrial membrane potential changes in cultured neurons. *J. Biol. Chem.* **281**, 14864–14874 (2006).
37. Erez, Y. et al. Comparative study of the photoprotolytic reactions of D-luciferin and oxyluciferin. *J. Phys. Chem. A* **116**, 7452–7461 (2012).
38. Wyatt, C. N. & Buckler, K. J. The effect of mitochondrial inhibitors on membrane currents in isolated neonatal rat carotid body type I cells. *J. Physiol.* **556**, 175–191 (2004).
39. Lou, P. H. et al. Mitochondrial uncouplers with an extraordinary dynamic range. *Biochem. J.* **407**, 129–140 (2007).
40. Manago, A. et al. Early effects of the antineoplastic agent salinomycin on mitochondrial function. *Cell Death Dis.* **6**, e1930 (2015).
41. Martens, C. R. et al. Chronic nicotinamide riboside supplementation is well-tolerated and elevates NAD^+ in healthy middle-aged and older adults. *Nat. Commun.* **9**, 1286 (2018).
42. Mouchiroud, L. et al. The NAD^+/Sirtuin pathway modulates longevity through activation of mitochondrial UPR and FOXO signaling. *Cell* **154**, 430–441 (2013).
43. Vannini, N. et al. The NAD-booster nicotinamide riboside potently stimulates hematopoiesis through increased mitochondrial clearance. *Cell Stem Cell* **24**, 405–418 (2019).
44. Lowell, B. B. & Spiegelman, B. M. Towards a molecular understanding of adaptive thermogenesis. *Nature* **404**, 652–660 (2000).
45. Cypess, A. M. et al. Activation of human brown adipose tissue by a β_3-adrenergic receptor agonist. *Cell Metab.* **21**, 33–38 (2015).
46. Virtanen, K. A. Activation of human brown adipose tissue (BAT): focus on nutrition and eating. *Handb. Exp. Pharmacol* **251**, 349–357 (2018).
47. Yang, Y. et al. Mitochondria and mitochondrial ROS in cancer: novel targets for anticancer therapy. *J. Cell. Physiol.* **231**, 2570–2581 (2016).
48. Schondorf, D. C. et al. The NAD^+ precursor nicotinamide riboside rescues mitochondrial defects and neuronal loss in iPSC and fly models of Parkinson's disease. *Cell Rep.* **23**, 2976–2988 (2018).
49. Szabadkai, G. & Duchen, M. R. Mitochondria mediated cell death in diabetes. *Apoptosis* **14**, 1405–1423 (2009).
50. Kleinert, M. et al. Animal models of obesity and diabetes mellitus. *Nat. Rev. Endocrinol.* **14**, 140–162 (2018).

Methods

General materials and methods. All chemicals for the in vitro and in vivo experiments were purchased from Sigma-Aldrich Chemie except for FCCP, which was purchased from Fluorochem. Earle's minimum essential medium (MEM), its supplements (100 mM sodium pyruvate, 1 M HEPES and non-essential amino acid solution), RPMI medium (ATCC modification) and PBS were purchased from Life Technologies. NR was purchased from ChromaDex. All plastic materials for cell culture (flasks for cell cultivation, serological pipettes and tubes) were purchased from Corning.

Chemical reagents. Procedures for the chemical synthesis and characterization of novel reagents are summarized in Supplementary Note 2. All chemicals for synthesis were purchased from the following commercial sources and used without further purification. 6-Hydroxybenzo[d]thiazole-2-carbonitrile was purchased from Endotherm. Diisopropylethylamine (DIPEA) and benzotriazol-1-yl-N-oxy-tris(pyrrolidino)phosphonium hexafluorophosphate (PyBOP) were purchased from Merck. 1-(3-Dimethylaminopropyl)-3-ethylcarbodiimide hydrochloride (EDC) was purchased from Thermo Fisher Scientific. Tris(2-carboxyethyl) phosphine hydrochloride (TCEP) was purchased from Fluorochem. All other reagents used for synthesis were purchased from Sigma-Aldrich Chemie.

Cell culture. All the cell lines used in this study were stably transfected with the luciferase gene and obtained from PerkinElmer. HT-1080-luc and HepG2-luc cells were transfected with the luc2 luciferase gene, and 4T1-luc cells were transfected with the Redluc luciferase gene. The HT-1080-luc and HepG2-luc cells were cultured in Earle's MEM supplemented with 10% (vol/vol) FBS, 1 mM sodium pyruvate, 0.1 mM non-essential amino acids and 10 mM HEPES. 4T1-luc cells were cultured in RPMI 1640 (ATCC modification) medium supplemented with 10% (vol/vol) FBS. The cells were maintained at 37 °C in a 5% CO_2 atmosphere until they reached 90–95% confluency and then were split in a ratio of 1:10.

For cell-based assays, the cells were plated (20,000 cells per well for HT-1080-luc and 4T1-luc or 30,000 cells per well for HepG2-luc) in a black, clear-bottomed 96-well plate (Becton Dickinson) and incubated at 37 °C with 100% humidity and 5% CO_2 for 24 h before an assay.

Measurement of S/B ratio of MAL probes. HT-1080-luc cells were first incubated with either TPP-CL1 or TPP-CL2 for 1 h and washed with PBS, followed by the addition of a 10 µM solution of either azido-TPP1 or azido-TPP2 and followed by continuous signal acquisition for 1 h. The resulting total photon flux was compared with the background levels (TPP-CL only) for all four MAL probes.

Measurement of cell viability by CellTiter Glo assay. HT-1080-luc cells seeded in 96-well plates were incubated with 100 µl solution of an azido-TPP or TPP-CL (various concentrations) in growing medium for 2 h at 37 °C. To each well of the plate, 100 µl of CellTiter Glo reagent (Promega) was added. After a 10-min incubation at room temperature, the luminescent signal was measured with an IVIS Spectrum system.

Measurement of cell viability by alamarBlue assay. AlamarBlue reagents were acquired from Thermo Fisher Scientific and the assay was performed according to the manufacturer&rsqo;s instructions. The alamarBlue reagent was diluted 11 times with solutions of an azido-TPP or TPP-CL (various concentrations) in growing medium (EMEM). Resulting mixtures were added on top of HT-1080 cells seeded in a 96-well plate. The cells were incubated with the solutions of azido-TPP or TPP-CL reagents for 2 h at 37 °C, followed by acquisition of fluorescent signal (ex. 545 nm; em. 580 nm) measured by a Tecan M1000 plate reader.

Measurement of an effect of MAL reagents on $\Delta\Psi_m$ levels with TMRM assay. HT-1080-luc cells were seeded in a 96-well plate 24 h prior to the assay at a density of 20,000 cells per well. Then, medium on top of the cells was exchanged with complete growth medium supplemented with 50 nM TMRM and either azido-TPP or TPP-CL (various concentrations). Cells were incubated at 37 °C for 1 h, washed once with PBS, and the fluorescence signal was measured using a Tecan M1000 plate reader.

Influence of MAL3 components on basal OCR. HT-1080-luc cells were seeded in XF96 cell culture microplates at a density of 20,000 cells per well with normal culture medium and allowed to attach overnight. Before the assay growing medium was exchanged to Krebs-Ringer bicarbonate HEPES buffer (KRBH) containing 5 mM glucose (pH 7.4). OCR was measured using a Seahorse XF96 analyzer (Agilent), Seahorse Wave software and Seahorse XF sensor cartridges. Three baseline measurements of OCR were taken before sequential injections of MAL3 components or effectors of ETC function. Each measurement cycle consisted of 2 min of mixing and 5 min of OCR measurement. Final concentrations for the ETC effectors are 1 µM for oligomycin, 3 µM for FCCP and 1 µM for both rotenone and antimycin A. To process raw data, we first subtracted non-mitochondrial respiration level from all readings. Then, relative respiration was calculated by assigning the average basal OCR to 100%. Finally, the difference between average basal OCR and each timepoint after addition of azido-TPP1 or TPP-CL2 was tested for statistical significance using two-way ANOVA with Dunnett's multiple comparisons test.

Effect of luciferin on $\Delta\Psi_m$ and ADP/ATP ratio in HT-1080-luc cells. The HT-1080-luc cells were incubated in growth medium comprising 50 nM TMRM and various concentrations of luciferin (0–10 µM) for 45 min, followed by a wash and fluorescent signal acquisition using a standard plate reader. Our results indicate that luciferin does not alter $\Delta\Psi_m$ levels at a concentration up to 10 µM.

ADP/ATP ratio was quantified with the commercially available kit from Abcam (ab65313). The HT-1080-luc cells were incubated in growth medium supplemented with various concentrations of luciferin (0–10 µM) for 45 min. We used the kit according to the manufacturer's instructions. In the tested concentration range we observed no effect of luciferin on the ADP/ATP ratio.

Monitoring of $\Delta\Psi_m$ in vitro with MAL and TMRM probes. *Detection of FCCP- or valinomycin-induced depolarization with the MAL3 probe.* Cells were incubated in culture medium containing 5 µM TPP-CL2 ± FCCP (0–3 µM)/valinomycin (0–30 nM) for 1 h at 37 °C. The cells were then washed once with 100 µl of PBS (1×). Next, a solution of azido-TPP1 (10 µM) and FCCP (0–3 µM)/valinomycin (0–30 nM) in growth medium was added to the cells. Immediately after this addition, the plate with the cells was placed in the chamber of an IVIS Spectrum system and imaged over 45 min, with one image acquired every minute (auto exposure). The AUC was integrated over 45 min and plotted as a bar graph (Fig. 2b,d and Supplementary Fig. 10).

Detection of nigericin-induced $\Delta\Psi_m$ hyperpolarization with MAL3 probe. In the experiments with the MAL3 probe, the cells were incubated in culture medium containing 5 µM TPP-CL2 ± nigericin (0–10 µM) for 1 h at 37 °C. The cells were washed once with 100 µl of PBS (1×). Next, a solution of azido-TPP1 (10 µM) and nigericin (0–10 µM) in growth medium was added to the cells. Immediately after this addition, the plate with the cells was placed in the chamber of an IVIS Spectrum system and imaged over 1 h, with one image acquired every minute (auto exposure). The AUC was integrated over 1 h and plotted as a bar graph (Fig. 2f and Supplementary Figs. 15a and 16).

Data processing. Images acquired with the IVIS Spectrum system were processed in Living Image 4.1 software (PerkinElmer) to quantify the bioluminescent signal observed over time from different groups. To obtain kinetic curves and integrate them, we used MS Excel 2016 (Microsoft) and GraphPad Prism 8.0.2 (GraphPad Software).

Fluorescent imaging of $\Delta\Psi_m$ in vitro with TMRM probe. The TMRM probe was used according to previously published procedures[51,52]. Similar to the experiments with the MAL1 and MAL3 probes, cells were incubated with solutions of TMRM (50 nM) ± FCCP (0–3 µM)/valinomycin (0–30 nM)/nigericin (0.5–10 µM) in growth medium for 1 h at 37 °C. The cells were washed once with 100 µl of PBS (1×), and the fluorescence signal from the 96-well plate was immediately acquired using a Tecan M1000 plate reader (ex. 535 nm; em. 560 nm) and Tecan i-Control 1.11 software. The data were analyzed using Microsoft Excel 2016 (Microsoft) and GraphPad Prism 8.0.2 (GraphPad Software).

Monitoring of $\Delta\Psi_p$. $\Delta\Psi_p$ was monitored using a membrane potential evaluation assay kit (cat. no. R8128, Molecular Devices). Briefly, HT-1080-luc cells were seeded in a 96-well plate 24 h before the assay, followed by incubation in 100 µl of a 1:1 mixture of the loading buffer with either EMEM or high-K^+ medium at 37 °C for 40 min. Then, 10 µl of an 11× effector solution (FCCP, valinomycin or nigericin) in EMEM was added to the wells and incubated at 37 °C for 50 min, followed by fluorescent signal acquisition according to the manufacturer's instructions using a Tecan M1000 (ex. 488 nm; em. 540–590 nm).

Contribution of $\Delta\Psi_p$ to the signal from MAL3 and TMRM. HT-1080-luc cells were first incubated in a 5 µM solution of TPP-CL2 in either low-K^+ or high-K^+ medium (Supplementary Table 3) for 50 min at 37 °C and then washed once with PBS. Next, a 10 µM solution of azido-TPP1 in either low-K^+ or high-K^+ medium was added to cells, followed by bioluminescent signal acquisition for 45 min using the IVIS Spectrum system.

A similar protocol was used to measure the contribution of $\Delta\Psi_p$ in the signal from TMRM. Briefly, HT-1080-luc cells were incubated in either low-K^+ or high-K^+ medium supplemented with 50 nM TMRM for 1 h, washed with PBS, then fluorescence intensity was measured with a Tecan M1000 plate reader.

Effect of ETC inhibition on the signal from MAL3 and TMRM. HT-1080-luc cells were incubated with 5 µM TPP-CL2 in growth medium supplemented either with vehicle or a mixture of antimycin A and oligomycin (10 µM and 7 µM, respectively) for 50 min followed by a washing step and subsequent addition of azido-TPP1 in the growth medium (10 µM) supplemented either with vehicle (DMA 0.1%) or a mixture of antimycin A and oligomycin (10 µM and 7 µM, respectively). The cells were then imaged continuously for 1 h using a CCD camera (IVIS100, PerkinElmer).

We used TMRM as a control because it is a gold standard in the field of $\Delta\Psi_m$ in vitro measurements. Briefly, HT-1080-luc cells were incubated in growth medium containing 50 nM TMRM and either vehicle (DMA 0.1%) or a mixture of antimycin A with oligomycin (10 µM and 7 µM, respectively) for 1 h. The cells were washed with PBS and the fluorescent signal from the cells was measured using a Tecan M1000 system.

Animal experiments. *Experimental animals.* Transgenic FVB-luc$^+$ mice were purchased from The Jackson Laboratory (full abbreviation: FVB-Tg[CAG-luc,-GFP] L2G85Chco/J). The breeding colony was housed in groups of four or five mice according to their age and gender. Swiss nude mice (Crl:NU(Ico)-Foxn1^{nu}) were purchased from Charles River Laboratories. The mice had free access to food (chow diet 3242, Kliba Nafag) and water, and were kept at 22 °C, 50% relative humidity, 75 air changes per hour, 65 lux illumination, and under a regular 12-h light–12-h dark cycle. All animal experiments were approved by the Veterinary Authority of Canton Vaud, Switzerland (license nos. 2849c and 3316b).

General procedure for imaging and monitoring of $\Delta\Psi_m$ in vivo. An IVIS Spectrum system was used for imaging and quantification of the bioluminescent signal in all animal experiments. The resulting data were processed using Living Image 4.1 software. In a typical experiment with the MAL3 probe, TPP-CL2 was first dissolved in dry DMF to a concentration of 30 mM. The resulting stock solution was further diluted 20 times with a solution of 0.1% BSA in PBS (1×) to a final concentration of 1.5 mM. Next, 100 µl of the resulting solution was injected i.v. into each FVB-luc$^+$ mouse in the control and sample groups. Twenty hours later, the mice received an i.p. injection of either 100 µl of a 15 mM azido-TPP1 solution in PBS (control group) or 100 µl of PBS (background group). Immediately after this, the mice were anesthetized with isoflurane, placed in the IVIS Spectrum chamber and imaged for 1 h. Images were acquired every minute using the following settings: exposure time auto, aperture F1, binning medium and field of view D. The total photon flux values were obtained by integration of the area under the kinetic curves and plotted in the form of bar graphs.

Studies of BHT-induced depolarization in vivo. Three groups of FVB-luc$^+$ mice ($n=3$) were first injected i.v. with TPP-CL2 solution (0.15 µmol, 100 µl in 0.1% BSA in PBS). Then, mice in group 1 received an oral gavage of BHT solution in corn oil (60 mg kg^{-1}, 200 µl), while those in groups 2 and 3 received only corn oil. Afer 20 h, mice in groups 1 and 2 were injected i.p. with azido-TPP1 (1.5 µmol in 100 µl of PBS), while those in group 3 (background) were injected with vehicle (PBS). Immediately after the injection, all mice were anesthetized and continuously imaged using an IVIS Spectrum system for 1 h. Images were acquired every minute using the following settings: exposure time auto, aperture F1, binning medium and field of view D. The total photon flux resulting from all three groups was integrated over 1 h and plotted as the S/B ratio of the signal obtained from the MAL3 BHT-treated group (group 1) or the group treated with MAL3 alone (group 2) normalized to the signal from the background (group 3, TPP-CL2 only).

Studies of nigericin-induced hyperpolarization in vivo. Three groups of FVB-luc$^+$ mice ($n=3$) received an i.v. injection of TPP-CL2 solution (0.15 µmol, 100 µl in 0.1% BSA in PBS); 20 h later, group 1 was injected with 100 µl of a solution containing nigericin (1.6 mg kg^{-1}, 640 µM) and azido-TPP1 (1.5 µmol in 0.1% BSA in PBS), group 2 was injected with azido-TPP1 only, and group 3 received a 100-µl injection of vehicle (0.1% BSA in PBS). Immediately after this injection, all mice were anesthetized and imaged using an IVIS Spectrum system continuously for 1 h. Images were acquired every minute using the following settings: exposure time auto, aperture F1, binning medium and field of view D. The total photon flux resulting from all three groups was integrated over 1 h and plotted as the S/B ratio of the signal obtained from the MAL3 nigericin-treated group (group 1) or the group treated with MAL3 alone (group 2) normalized to the signal from the background (group 3, TPP-CL2 only).

Impact of BHT and nigericin on oxygen consumption of FVB-luc$^+$ mice. Oxygen consumption was measured using the Promethion high definition multiplexed respirometry system for mice (Sable Systems International). In a typical experiment, a group of 9 or 10 FVB-luc$^+$ mice were placed in metabolic cages (one mouse per cage) on day 0 of the study and recordings of various parameters, e.g. rate of oxygen consumption (V_{O_2}), rate of carbon dioxide emission (V_{CO_2}), rate of water vapor loss (V_{H_2O}), respiratory quotient (RQ), energy expenditure (EE), locomotion and so on, was started immediately. On the fourth day the mice received corresponding vehicle (corn oil by oral gavage or PBS by i.p. injection). At 24 h later, a solution of either BHT or nigericin was administered to all mice. BHT (60 mg kg^{-1}) solution in corn oil was given by oral gavage and nigericin (3.2 mg kg^{-1}) solution in PBS supplemented with 0.1% BSA was administered by i.p. injection. Recording was stopped 24 h after administration of BHT and nigericin. The data were processed using ExpeData software provided by the manufacturer of the Promethion high definition multiplexed respirometry system.

Studies of age-related $\Delta\Psi_m$ depolarization in vivo. We compared 12-week-old FVB-luc$^+$ female mice ('young' group) with 65-week-old mice ('old' group) of the same FVB-luc$^+$ strain ($n=4$). On the first day of the experiment, all mice received i.v. injections of TPP-CL2 (5 mg kg^{-1}, 100 µl in 0.1% BSA in PBS) and were placed back in their cages. On the second day (20 h later), the mice were imaged for 30 min using a CCD camera, followed by an i.p. injection of azido-TPP1 (1.5 µmol in 100 µl of PBS) and subsequent imaging for another 40 min. The total photon flux resulting from the injection of azido-TPP1 was normalized to the total photon flux resulting from the injection of TPP-CL2 (background, first 30 min of imaging).

Clearance of TPP-CL2 from plasma of old and young FVB-luc$^+$ mice. Nine 83–85-week-old ('old' group) and nine 26–28-week-old ('young' group) FVB-luc$^+$ female mice were injected i.v. with TPP-CL2 solution (100 µl, 0.15 µmol in 0.1% BSA in PBS). At 15 min, 12 h and 20 h post-injection, three mice from each group were used for blood collection by heart puncture. The obtained samples were centrifuged (4° C, 5,000 r.c.f., 5 min) to separate plasma, then 50 µl of each plasma sample was mixed with an equal volume of 1 mM azido-TPP1 solution in PBS in a 96-well plate. The plate was incubated at room temperature for 2 h to let the reaction take place. Next, 10 µl of solution containing 10 mM ATP, 10 mM $MgSO_4$ and 80 µg ml^{-1} luciferase enzyme was added to each well of the plate. Immediately after this addition, the plate was placed in the chamber of an IVIS Spectrum system and imaged over 1 h, with one image acquired every minute (auto exposure). The AUC was integrated over 1 h and used to calculate the relative concentration of TPP-CL2. The average AUC of the samples collected 15 min post i.v. injection of TPP-CL2 was set to 1.0.

Measurement of mtDNA/nuDNA in young and old mice. Four old (>90 weeks) and six young (13 weeks) FVB-luc$^+$ mice fed with regular chow diet (3242, Kliba Nafag) were used for the experiment. The mice were euthanized to dissect heart, liver, kidneys and skeletal muscles. The organs were immediately frozen in liquid nitrogen and stored at −80 °C before being ground using a mortar and pestle in liquid nitrogen, then the resulting powder was lyophilized and stored at −30 °C before the assay. Genomic and mitochondrial DNA were isolated using a commercial Nucleo Spin Tissue kit (Macherey-Nagel) according to the manufacturer's instructions. Prior to quantitative PCR (qPCR) analysis, the isolated DNA was stored at −30 °C.

Real-time qPCR analysis was performed using primers for mtco-1 and atp-5 genes (Supplementary Table 2), PowerUp SYBR green master mix (Thermo Fisher) and QuantStudio 6 PCR system (Thermo Fisher). DNA primers were designed using Primer Express 3.0 software. The raw data were analyzed using QuantStudio Real-Time PCR Software (version 1.3, AppliedBiosystems). Fold changes of mtDNA/nDNA were calculated using the $2^{-\Delta\Delta CT}$ method[53].

Effect of NR-enriched diet on mtDNA/nuDNA in old mice. Ten old FVB-luc$^+$ mice (>90 weeks) were used to form three groups: group 1 (control, $n=4$) was fed control diet (2916, Teclad) for 14 days; group 2 was fed NR-enriched diet for seven days ($n=3$); group 3 was fed NR-enriched diet for seven days and then with the control diet for another seven days ($n=3$). At the end of the diet study, the mice were euthanized following by heart, liver, kidneys and skeletal muscle dissection (Supplementary Fig. 27a). Isolation of DNA from the organs, qPCR analysis and calculation of mtDNA/nuDNA ratio were performed as described above in the section 'Measurement of mtDNA/nuDNA in young and old mice'.

Preparation of NR-enriched and control diets. A 3.8 g sample of NR triflate powder (2.4 g of NR) was dissolved in 400 ml of sterile water. The resulting solution was mixed with 1 kg of irradiated powder chow diet (2916, Teclad) to reach a final concentration of NR at 0.24% of mixture mass. The mixture was well homogenized and divided into pellets of 10–15 g. The pellets were dried at room temperature and stored at −80 °C. Each day, new pellets were given to the mice.

Effect of NR-enriched diet on $\Delta\Psi_m$ in old FVB-luc$^+$ mice. A group of five FVB-luc$^+$ 90–95-week-old female mice was used for this study. The mice were fed an NR-enriched diet for seven days continuously. Each day, a fresh portion (50–55 g) of the NR-enriched diet was given to the mice. On the eighth day, the mice were switched to the control diet (2916, Teclad). $\Delta\Psi_m$ values were measured in exactly the same way as described previously (section 'Studies of age-related $\Delta\Psi_m$ depolarization in vivo'). The measurements were performed a day before the start of the NR-enriched diet (day 0), immediately after the diet (day 7), one week after the NR diet (day 14) and two weeks after the NR diet (day 21).

Effect of NR-enriched diet on the activity of luciferase in FVB-luc$^+$ mice. A group of five 90-week-old female mice was fed an NR-enriched diet for seven days continuously in the same way as described above. On the eighth day, the mice were switched to control diet (2916, Teclad). At days 0, 7 and 14, these mice were injected i.p. with 200 µl of 100 mM luciferin solution and then imaged in an IVIS Spectrum system (exposition auto, binning 8, F1, field of view D) continuously for 1 h.

Assessing mitochondrial depolarization in BAT induced by CL316,243. Two groups of 15-week-old FVB-luc$^+$ mice ($n=5$) were injected i.v. with TPP-CL2 (100 µl, 0.15 µmol in 0.1% BSA in PBS), followed by i.p. injection of CL solution (100 µl, 1 mg kg^{-1} in PBS) or PBS alone 19 h later. After that, the mice from both groups received i.p. injections of azido-TPP1 solution (100 µl, 1.5 µmol in PBS) followed by

euthanasia and isolation of BAT 50 min post-injection. The tissues were placed on a Petri dish and imaged in an IVIS Spectrum system (exposition auto, binning 8, F1, field of view D).

Non-invasive monitoring of $\Delta\Psi_m$ in animal cancer models. A group of eight-week-old female Swiss nude mice ($n=5$) were inoculated with one million 4T1-luc cells subcutaneously in the left flank. The size of the tumor was carefully monitored and, on the ninth day post-inoculation, the tumors had grown to a volume of 0.5–0.6 cm^3. The mice received an i.v. injection of 100 µl of 1 mM solution of TPP-CL2 in PBS supplemented with 0.1% BSA (day 0). After 20 h, the animals were injected i.p. with 100 µl of 15 mM solution of azido-TPP1 in PBS and subsequently imaged for 30 min using the IVIS Spectrum. After this imaging session with the MAL3 probe, the mice received an i.p. injection of 100 µl of a 100 mM luciferin solution in PBS followed by another 30 min of imaging to control for their tumor size (day 1).

The mice were allowed to rest for two days to make sure they did not have any remaining signal. Two days later the experiment was repeated in the presence of nigericin—a potent widely used $\Delta\Psi_m$ hyperpolarizer. The mice first received an i.v. injection of TPP-CL2 (day 3) followed by an i.p. injection of 100 µl of solution containing 15 mM azido-TPP1 and 600 µM nigericin. Immediately afterwards, the mice were imaged in an IVIS Spectrum for 30 min. After this imaging session with MAL3, the mice received an i.p. injection of 100 µl of 100 mM luciferin solution in PBS and were imaged again for 30 min to control for tumor size (day 4). The resulting total photon flux from MAL3 probe without (day 1) and with nigericin (day 4) was divided (normalized) by the total photon flux from luciferin injection obtained the same day. This normalization was done to account for differences in tumor size between animals.

Statistical analysis. Quantitative data are presented as mean ± s.d., if not stated otherwise. Each experiment was repeated two or more times unless stated otherwise. Differences were compared using Student's *t*-test or one-way ANOVA. When *P* values were 0.05 or less, the differences were considered statistically significant. The value of the Z' factor was calculated according to

$$Z' = 1 - \frac{3(\sigma_{pos} + \sigma_{neg})}{\bar{X}_{pos} - \bar{X}_{neg}}$$

where σ_{pos} and σ_{neg} are the standard deviations for the positive and negative groups, respectively, and $\bar{X}_{pos}$ and $\bar{X}_{neg}$ are the mean values for the positive and negative groups, respectively.

Reporting Summary. Further information on research design is available in the Nature Research Reporting Summary linked to this Article.

Data availability

The data that support the findings of this study are available from the corresponding author upon request. CCDC nos. 1940412, 1940411, 1940410 and 1940409 for compounds **7**, **9**, **13** and **16**, contain the supplementary crystallographic data for this paper. These data can be obtained, free of charge, from The Cambridge Crystallographic Data Centre via www.ccdc.cam.ac.uk/structures.

References

51. Zha, L. et al. The histone demethylase UTX promotes brown adipocyte thermogenic program via coordinated regulation of H3K27 demethylation and acetylation. *J. Biol. Chem.* **290**, 25151–25163 (2015).
52. Erlich-Hadad, T. et al. TAT-MTS-MCM fusion proteins reduce MMA levels and improve mitochondrial activity and liver function in MCM-deficient cells. *J. Cell. Mol. Med.* **22**, 1601–1613 (2018).
53. Livak, K. J. & Schmittgen, T. D. Analysis of relative gene expression data using real-time quantitative PCR and the $2^{-\Delta\Delta CT}$ method. *Methods* **25**, 402–408 (2001).

Acknowledgements

We thank the EPFL NMR facility staff and especially P. Mieville for help with acquiring 2D spectra, the EPFL XRD facility staff for help with crystal structure determination, and the EPFL MS facility for help with HRMS measurements. We thank O. Naveiras and A. Oggier (ISREC, EPFL), who kindly provided NR-enriched and control diets. We also thank G. Karateev for help and advice regarding the synthesis of TPP-CL2. We appreciate the help of R. Combe and M. Kulagin, members of the CPG facility at EPFL, in measuring the oxygen consumption by mice. We thank the Swiss National Foundation (grant no. 31003A_150134) for funding this work.

Author contributions

E.A.G. conceptualized the study and acquired the funding. E.A.G. and A.A.B. designed the experiments. A.A.B., R.S. and N.S. synthesized the compounds. A.A.B. performed the experiments and analyzed the data. A.A.B., A.H. and U.D.M. designed and performed cellular OCR measurements. T.M. measured the clearance of TPP-CL2 in vivo, and designed and drew the graphical abstract. G.B. assisted in measurement of the nigericin effect in cells with TMRM. E.A.G. and A.A.B. wrote the manuscript. All authors edited the manuscript.

Competing interests

The authors declare no competing interests.

Additional information

Supplementary information is available for this paper at https://doi.org/10.1038/s41589-020-0602-1.

Correspondence and requests for materials should be addressed to E.A.G.

Reprints and permissions information is available at www.nature.com/reprints.

nature research

Corresponding author(s): Elena Goun

Last updated by author(s): Jun 1, 2020

Reporting Summary

Nature Research wishes to improve the reproducibility of the work that we publish. This form provides structure for consistency and transparency in reporting. For further information on Nature Research policies, see our Editorial Policies and the Editorial Policy Checklist.

Statistics

For all statistical analyses, confirm that the following items are present in the figure legend, table legend, main text, or Methods section.

n/a	Confirmed
☐	☒ The exact sample size (*n*) for each experimental group/condition, given as a discrete number and unit of measurement
☐	☒ A statement on whether measurements were taken from distinct samples or whether the same sample was measured repeatedly
☐	☒ The statistical test(s) used AND whether they are one- or two-sided *Only common tests should be described solely by name; describe more complex techniques in the Methods section.*
☒	☐ A description of all covariates tested
☐	☒ A description of any assumptions or corrections, such as tests of normality and adjustment for multiple comparisons
☐	☒ A full description of the statistical parameters including central tendency (e.g. means) or other basic estimates (e.g. regression coefficient) AND variation (e.g. standard deviation) or associated estimates of uncertainty (e.g. confidence intervals)
☐	☒ For null hypothesis testing, the test statistic (e.g. *F*, *t*, *r*) with confidence intervals, effect sizes, degrees of freedom and *P* value noted *Give P values as exact values whenever suitable.*
☒	☐ For Bayesian analysis, information on the choice of priors and Markov chain Monte Carlo settings
☒	☐ For hierarchical and complex designs, identification of the appropriate level for tests and full reporting of outcomes
☒	☐ Estimates of effect sizes (e.g. Cohen's *d*, Pearson's *r*), indicating how they were calculated

Our web collection on statistics for biologists contains articles on many of the points above.

Software and code

Policy information about availability of computer code

Data collection	Living Image 4.1, Tecan i-Control 1.11, Applied Biosystems QuantStudio 1.3, Seahorse Wave, Brucker TopSpin 4.1, ShelXT.
Data analysis	Living Image 4.1, Applied Biosystems QuantStudio 1.3, Microsoft Excel 2016, GraphPad Prism 8.0.2, MestReNova 12.0.0-20080, ShelXT, ExpeData.

For manuscripts utilizing custom algorithms or software that are central to the research but not yet described in published literature, software must be made available to editors and reviewers. We strongly encourage code deposition in a community repository (e.g. GitHub). See the Nature Research guidelines for submitting code & software for further information.

Data

Policy information about availability of data

All manuscripts must include a data availability statement. This statement should provide the following information, where applicable:

- Accession codes, unique identifiers, or web links for publicly available datasets
- A list of figures that have associated raw data
- A description of any restrictions on data availability

The data that support the findings of this study are available from the corresponding author upon request. CCDC numbers 1940412, 1940411, 1940410, 1940409 for compounds 7, 9, 13, and 16, contain the supplementary crystallographic data for this paper. These data can be obtained, free of charge, from The Cambridge Crystallographic Data Centre via www.ccdc.cam.ac.uk/structures.

Field-specific reporting

Please select the one below that is the best fit for your research. If you are not sure, read the appropriate sections before making your selection.

☒ Life sciences ☐ Behavioural & social sciences ☐ Ecological, evolutionary & environmental sciences

For a reference copy of the document with all sections, see nature.com/documents/nr-reporting-summary-flat.pdf

Life sciences study design

All studies must disclose on these points even when the disclosure is negative.

Sample size	Group size for original data created here was based on previous experience. No statistical method was used to predetermine sample size.
Data exclusions	No data were removed from analysis
Replication	All presented results were successfully reproduced at least twice. Measurement of oxygen consumption by mice was performed once.
Randomization	Allocation of mice to experimental groups was random
Blinding	Data collection and Analysis was not performed blind.

Reporting for specific materials, systems and methods

We require information from authors about some types of materials, experimental systems and methods used in many studies. Here, indicate whether each material, system or method listed is relevant to your study. If you are not sure if a list item applies to your research, read the appropriate section before selecting a response.

Materials & experimental systems

n/a	Involved in the study
☒	☐ Antibodies
☐	☒ Eukaryotic cell lines
☒	☐ Palaeontology and archaeology
☐	☒ Animals and other organisms
☒	☐ Human research participants
☒	☐ Clinical data
☒	☐ Dual use research of concern

Methods

n/a	Involved in the study
☒	☐ ChIP-seq
☒	☐ Flow cytometry
☒	☐ MRI-based neuroimaging

Eukaryotic cell lines

Policy information about cell lines

Cell line source(s)	All cell lines used in this study, i.e. HT-1080-luc, 4T1-luc, HepG2-luc, were purchased from PerkinElmer (USA)
Authentication	None of the cell lines were authenticated.
Mycoplasma contamination	Cell lines were tested with the MycoProbe kit(R&D Systems) and results were negative for mycoplasma contamination.
Commonly misidentified lines (See ICLAC register)	No commonly misidentified cell lines were used

Animals and other organisms

Policy information about studies involving animals; ARRIVE guidelines recommended for reporting animal research

Laboratory animals	Swiss nude mice (Crl:NU(Ico)-Foxn1nu), females, 8 weeks old purchased from Charles River FVB-Tg[CAG-luc,-GFP]L2G85Chco/J mice, both sexes, 5-8 weeks old were purchased from Jackson laboratory. Breeding colony was established according to Swiss Cantonal Veterinary Office rules and regulations.
Wild animals	No wild animals were used
Field-collected samples	No field samples were acquired for this study
Ethics oversight	All animal experiments were approved by the Veterinary Authority of the Canton Vaud, Switzerland (Licenses #2849c, 3316b).

Note that full information on the approval of the study protocol must also be provided in the manuscript.